

Fading Light, Fierce Winds: JWST Snapshot of a Sub-Eddington Quasar at Cosmic Dawn

JIANWEI LYU (吕建伟) ¹, GEORGE H. RIEKE ¹, MEREDITH STONE ¹, JANE MORRISON ¹, STACEY ALBERTS ¹,
XIANGYU JIN ¹, YONGDA ZHU ¹, WEIZHE LIU (刘伟哲) ¹ AND JINYI YANG ²

¹Steward Observatory, University of Arizona, 933 North Cherry Avenue, Tucson, AZ 85721, USA

²Department of Astronomy, University of Michigan, 1085 S. University Ave., Ann Arbor, MI 48109, USA

ABSTRACT

The majority of most luminous quasars during the epoch of reionization accrete near or above the Eddington limit, marking the vigorous growth of primitive supermassive black holes (SMBHs). However, their subsequent evolution and environmental impact remain poorly characterized. We present JWST/NIRSpec prism IFU observations of HSC J2239+0207, a low-luminosity quasar at $z \sim 6.25$ likely in a late stage of mass assembly with an overmassive SMBH relative to its host galaxy. Using $H\beta$ and $H\alpha$ broad emission lines, we estimate an SMBH mass $M_{\text{BH}} \sim 3 \times 10^8 M_{\odot}$ and confirm its sub-Eddington accretion at $\lambda_{\text{Edd}} \sim 0.4$. Strong Fe II emission and a proximity zone of typical size suggest a metal-rich, highly evolved system. In the far-UV, this quasar presents strong broad-absorption-line features, indicative of high-velocity winds ($v \sim 10^4$ km/s). Meanwhile, minimal dust reddening is inferred from the quasar continuum and broad-line Balmer decrement, suggesting little dust along the polar direction. Most interestingly, we identify a gas companion ~ 5 kpc from the quasar with a high $[\text{O III}]/H\beta$ ratio ($\gtrsim 10$), likely representing outflowing gas blown away by AGN feedback. These results highlight HSC J2239+0207 as a likely fading quasar in transition, providing rare insights into SMBH evolution, AGN feedback, and AGN-galaxy interactions in the early Universe.

1. INTRODUCTION

In the local Universe, correlations between the masses of supermassive black holes (SMBHs) and the properties of their host galaxies have been well established, postulating a possible co-evolution of SMBH and galaxy (e.g., see review by Kormendy & Ho 2013). Over the past two decades, characterizing and interpreting the relation between SMBHs and their hosts across cosmic time have been a key mission in extragalactic astronomy (e.g., Alexander & Hickox 2012; Heckman & Best 2014; Somerville & Davé 2015). The situation in the epoch of reionization ($z \sim 6$) has attracted particular interest. Observations of luminous quasars at these redshifts reveal SMBHs with masses exceeding $10^9 M_{\odot}$, providing a unique window into the early growth of SMBHs and the build-up of their host galaxies when the Universe was less than 1 Gyr old (e.g., see a recent review by Fan et al. 2023).

With unprecedented sensitivity, spatial resolution, and spectral coverage at near- to mid-IR wavelengths, JWST follow-up observations of these bright quasars have provided valuable insights into the quasar evolution, host galaxy properties and large-scale environment during the reionization

epoch (e.g., Ding et al. 2023; Yang et al. 2023; Wang et al. 2023; Stone et al. 2024). These most luminous quasars are found to be accreting at or above the Eddington limit (e.g., Fan et al. 2023) and the AGNs are metal-rich (e.g., Jiang et al. 2024) with identical spectral properties to their low- z counterparts (e.g., Yang et al. 2023). Compared to the masses of the SMBHs, the host galaxies are typically undermassive (e.g., Stone et al. 2024; Yue et al. 2024) and reside in overdense environments (e.g., Wang et al. 2023; Eilers et al. 2024). In theory, with the consumption of the surrounding materials, these quasars are expected to fade away with time and leave some signatures of the AGN feedback in the environment (e.g., Hopkins et al. 2008). Nevertheless, such phenomena are poorly characterized by observations.

In this paper, we present the JWST/NIRSpec IFU observations of HSC J2239+0207, an intriguing quasar at $z \sim 6.25$ discovered by the Subaru High- z Exploration of Low-Luminosity Quasars project (Izumi et al. 2019). Compared to other bright quasars at $z \gtrsim 6$, the luminosity of J2239+0207 is relatively low ($M_{1450, \text{optical}} = -24.7$ or $L_{\text{bol}} \sim 2.5 \times 10^{12} L_{\odot}$) and near the break of the quasar luminosity function at $z \sim 6$ (Matsuoka et al. 2018), making it more representative of the general quasar population during the reionization epoch. Ground-based spectral follow-up of this object put a tight constraint on the object redshift at $z=6.2498$ and a black hole mass estimate of $M_{\text{BH}} \sim (0.6 - 1) \times 10^9 M_{\odot}$

(based on MgII and CIV line widths; [Onoue et al. 2019](#)) with a corresponding Eddington ratio of $\sim 20\%$. Based on careful PSF subtractions of multi-band JWST/NIRCam medium band images of this quasar, [Stone et al. \(2023\)](#) reported the detection of the host galaxy stellar output and estimated a total stellar mass of $\sim 10^{10} M_{\odot}$. Combined with the SMBH mass measurement, this yields a black hole to galaxy stellar mass ratio ~ 15 times larger than predicted by the local $M_{\text{BH}}-M_{*}$ relation. The combination of the low Eddington ratio and over-massive nature of the SMBH indicates that HSC J2239+0207 is likely in a late stage of mass assembly. That is, as its accretion decreases and it gradually fades, its host galaxy is expected to grow continuously so the system will eventually approach more closely the typical $M_{\text{BH}}-M_{*}$ relation. Therefore, it offers us a unique opportunity to study SMBH evolution and AGN-galaxy interaction at cosmic dawn.

We organize this paper as follows: Section 2 describes the NIRSpec/IFU data reduction and the methods used for spectral analysis. In Section 3, we provide various constraints on the quasar properties, including e.g., the black hole mass, quasar proximity zone, iron emission strength, broad absorption lines, dust attenuation. Section 4 reports the discovery of a gas companion near the quasar redshift and characterizes its properties. Section 5 discusses the evolutionary stage of this system, the possible nature of the gas companion and the implication of our findings. We conclude with a final summary in Section 6. Throughout this paper, we adopted a cosmology with $H_0 = 69.6$, $\Omega_M = 0.286$, and $\Omega_{\Lambda} = 0.714$.

2. DATA REDUCTION AND ANALYSIS

2.1. Observation and Data Reduction

HSC J2239+0207 was observed with the NIRCam imager and NIRSpec IFU as part of the US MIRI GTO program 1205 (PI: George Rieke). The NIRCam results and a preliminary analysis of the NIRSpec quasar spectrum have been published in [Stone et al. \(2023\)](#). This paper focuses on the detailed analysis of the NIRSpec datacube.

The NIRSpec IFU data of HSC J2239+0207 were obtained on Nov 11, 2022 with the PRISM/CLEAR disperser-filter combination, providing a $3'' \times 3''$ data cube over a wavelength range of $0.6\text{--}5.3 \mu\text{m}$ (corresponding to $825\text{--}7300\text{\AA}$ at the quasar redshift) at a spectral resolution of $30\text{--}300$. A four-point dithering pattern was adopted to mitigate detector artifacts and cosmic rays and the total exposure time on source was about 2.5 hours.

We processed the NIRSpec data with JWST pipeline version 1.12.0 and the CRDS pipeline parameter reference file `jwt_1088.pmap` following the standard steps. This includes the first stage, *Detector1Pipeline*, to apply detector-level corrections (e.g., dark current and bias subtraction, persistence correction, cosmic-ray removal) to the raw data of individ-

ual exposures and produce the un-calibrated 2D spectra; and the second stage, *Spec2Pipeline*, to assign world coordinate system (WCS) information to the data, apply flat-field corrections, carry out flux calibration, and construct 3D data cubes from the 2D spectra obtained at each dither location. The third stage, *Spec3Pipeline*, combines the individual data cubes at different dither positions to produce the final merged data cube with outlier rejections, drizzling, etc. to remove any additional artifacts and improve spatial sampling. We found that the default pipeline did not always remove obvious outliers and added a customized step to mask out the bad pixels in the 2D spectra manually after a careful visual inspection of individual spectral slices. After this process, we re-constructed a final IFU cube for science analysis.

2.2. Spectrum Extraction and Fittings

To extract the unresolved nuclear quasar spectrum, we adopt a circular aperture at a radius of $0.35''$ across all wavelengths. For the background subtraction, we placed the same aperture at random locations of the cube that do not contain real structures, computed the medium background spectrum, and subtracted it from the quasar spectrum. We have used WebbPSF ([Perrin et al. 2014](#)) to simulate the wavelength-dependent instrument PSF and computed the required aperture corrections. Our aperture is large enough that the introduced maximum color offset is less than 8% across the whole wavelength range. In Figure 1, we present the nuclear spectrum of HSC J2239+0207 and compare it to a low-redshift quasar template that has been smoothed to the NIRSpec prism resolution, which will be discussed in the following section.

To decompose the quasar spectrum, we have adopted PyQSOFit ([Guo et al. 2018](#)) and conducted the spectral fittings in two wavelength windows: (1) the UV part from rest-frame 1700\AA to 3100\AA , and (2) the optical part from rest-frame 4400\AA to 7050\AA . First, the continuum was fitted with a power-law plus FeII templates ([Boroson & Green 1992](#); [Vestergaard & Wilkes 2001](#)) after masking out regions contributed by emission lines. Then we subtracted the continuum models from the observed spectra to get the emission-line only spectra. We have adopted three Gaussians to model the broad-line components and one Gaussian to model the narrow components. The fitting results are plotted in Figure 2.

As described later, there is an elongated emission line gas companion detected in the datacube. We extracted its signals with a rectangular aperture of $0.6'' \times 1''$ that covers the spatial distribution, and we subtracted the background emission in a similar way to the nuclear quasar spectrum. The emission lines from the companion are not broadened, so a single Gaussian is adopted to fit the emission lines, including the unresolved $\text{H}\alpha + [\text{N II}]$ complex.

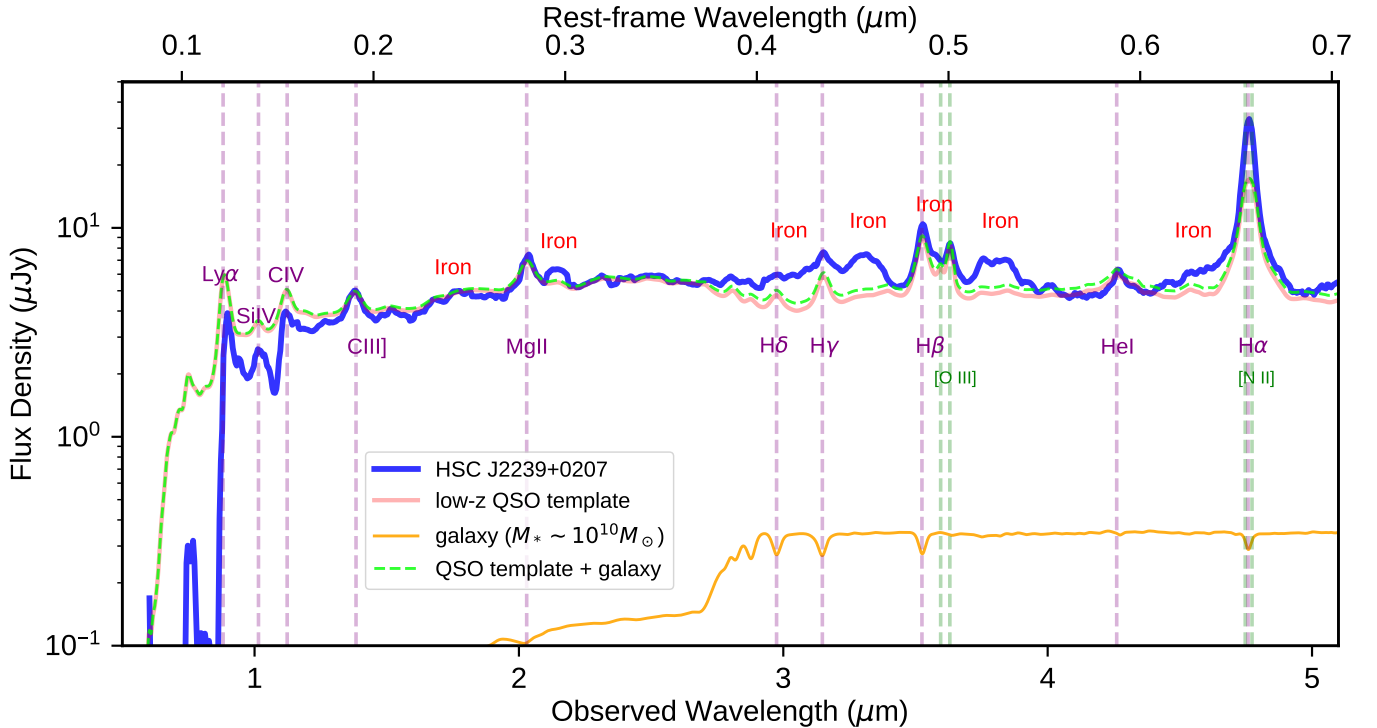


Figure 1. The observed nuclear quasar spectrum of HSC J2239+0207 (blue line). A normal quasar template built from SDSS is also plotted in red as a comparison. We have highlighted various spectral features. We have plotted a galaxy template with stellar mass $M_* \sim 10^{10} M_\odot$ (orange line) and show the resulting QSO+galaxy spectrum (green dashed line). All the templates have been smoothed to match the NIRSpc prism resolutions.

3. QUASAR PROPERTIES

Before diving into the detailed spectral analysis, we first compare the observed UV-to-optical spectrum of HSC J2239+0207 to quasars at low redshift. Although the quasar template from [Vanden Berk et al. \(2001\)](#) has been widely adopted as the reference to trace evolution at high- z , it does have notable contamination from the host galaxy (e.g., Ca II and Na I absorptions) and evidence for dust reddening. We have constructed a new quasar template from the Sloan Digital Sky Survey (SDSS) Quasar Catalog DR7 ([Schneider et al. 2010](#)) by combining the spectra of the 350 quasars with the bluest continuum and minimum stellar contamination. In Figure 1, we compare the spectrum of HSC J2239+0207 to this quasar template with the latter smoothed to match the JWST/NIRSpc prism resolution.

It turned out J2239+0207 is remarkably similar to this low- z template in terms of the continuum shape for the Fe II-free regions and the profiles of most emission lines. There are three notable differences: (1) boosted Fe II emission from the UV to the optical; (2) evidence of broad-line-absorptions at wavelengths shorter in the UV and strong Ly α absorption; (3) asymmetric profile of the H α + [N II] complex.

We describe the details of various quasar properties below.

3.1. Black Hole Mass and Eddington Ratio

With the decomposition of AGN emission lines (broad/narrow components from different atoms/ions) and underlying continuum (Fe II features, Balmer continuum, and AGN power-law), we can get reliable constraints on the mass of SMBHs from broad Balmer emission lines.

For H β , we adopt black hole mass estimator in [Vestergaard & Peterson \(2006\)](#)

$$\frac{M_{\text{BH}, \text{H}\beta}}{M_\odot} = 10^{6.91} \left(\frac{\text{FWHM}(\text{H}\beta)}{1000 \text{ km s}^{-1}} \right)^2 \left(\frac{\lambda L_\lambda(5100\text{\AA})}{10^{44} \text{ erg s}^{-1}} \right)^{0.5} \quad (1)$$

We measured the full-width half-maximum (FWHM) of the broad H β component to be 3019 km/s, after correcting for the instrument broadening (2244.8 km/s) from the apparent H β FWHM (3762.3 km/s). The 5100 \AA luminosity is measured to be 2.04×10^{45} erg/s and the resulting black hole mass is $3.34 \times 10^8 M_\odot$.

For H α , [Greene & Ho \(2005\)](#) provided a BH mass estimator based on the broad H α emission line alone.

$$\frac{M_{\text{BH}, \text{H}\alpha}}{M_\odot} = 10^{6.30} \left(\frac{\text{FWHM}(\text{H}\alpha)}{1000 \text{ km s}^{-1}} \right)^{2.06} \left(\frac{L_{\text{H}\alpha}}{10^{42} \text{ erg s}^{-1}} \right)^{0.55} \quad (2)$$

We measured the FWHM of the broad H α component to be ~ 3284 km/s after taking out the instrument broadening

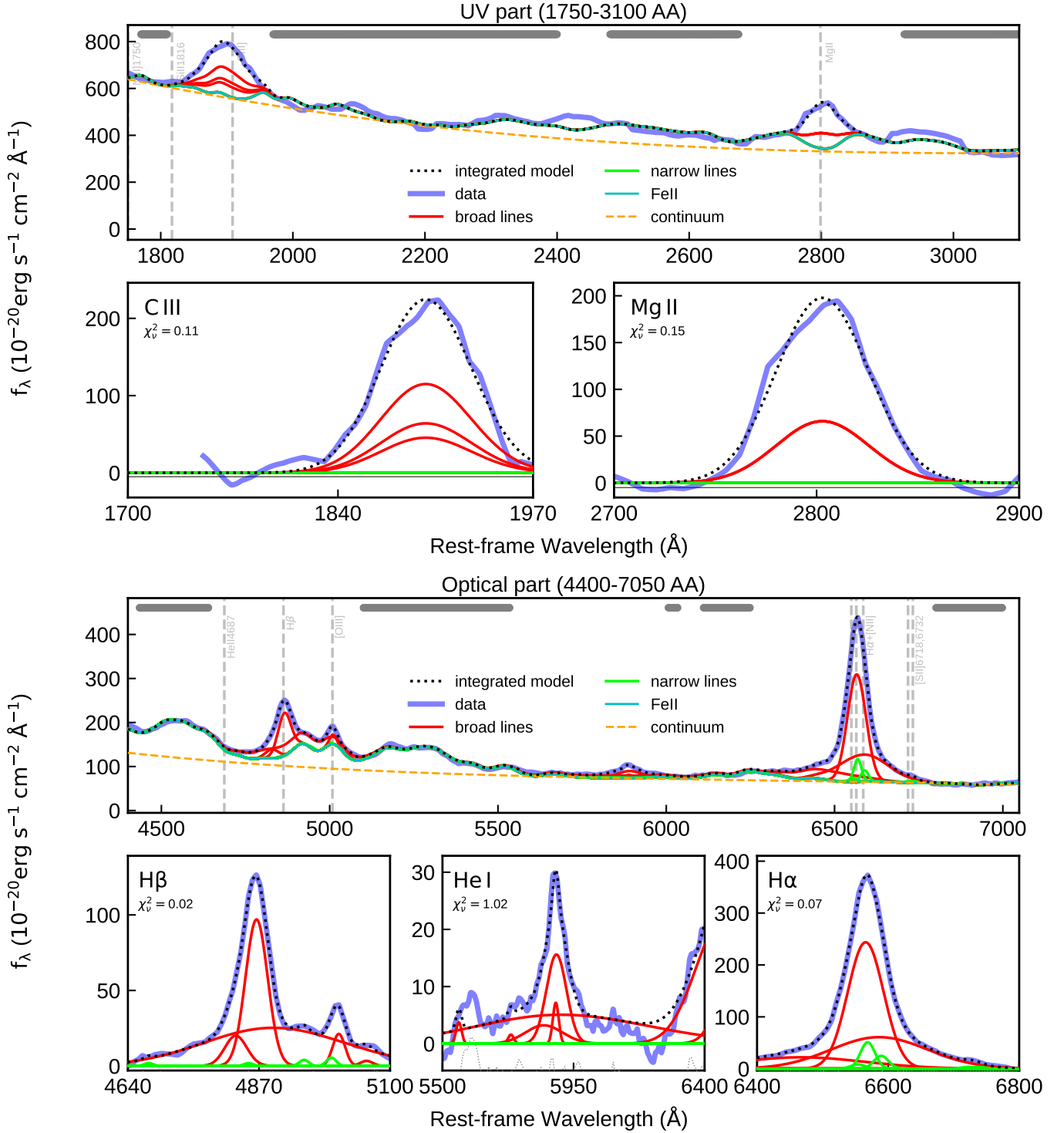


Figure 2. PyQSOFit spectral decomposition results of the UV (top) and optical bands (bottom) of HSC J2239+0207 NIRS pec prism spectrum. The integrated model (black dots) is composed of the AGN power-law continuum (dashed orange line), the iron emission model (thin blue line), the broad line components (red lines) and narrow line components (yellow lines). The data is shown in thick light blue line. The wavelengths of some strong nebular emission lines are labeled with vertical gray dashed lines and the gray horizontal bands on the top indicate the wavelength window used to fit the power-law continuum and iron models.

1163.9 km/s from the apparent FWHM of 3484.5 km/s. The $H\alpha$ luminosity is measured to be 1.41×10^{44} erg/s, thus the black hole mass based on broad $H\alpha$ is $3.51 \times 10^8 M_\odot$.

At shorter wavelengths, the spectral resolution of the prism data is too poor (~ 6019 km/s for CIII, ~ 9482 km/s for Mg II) to allow useful constraints on the black hole mass. We note that [Onoue et al. \(2019\)](#) reported the FWHM of MgII to be 4670_{-700}^{+910} km/s based on ground-based near-IR observations and estimated a MgII-based black hole mass $1.1_{-0.2}^{+0.3} \times 10^9 M_\odot$, which is about three times larger than the results from $H\alpha$ and $H\beta$. Similarly, they found a FWHM for CIV of 4630_{-1260}^{+1040} km/s leading to a black hole mass estimate of $6.3_{-2.5}^{+2.0} \times 10^8 M_\odot$, twice our estimate from $H\alpha$ and $H\beta$, but consistent within the large error. The differences are not atypical for single-epoch black hole mass estimates, and MgII and CIV specifically may be affected by winds; also the signal to noise of the [Onoue et al. \(2019\)](#) line measurements is low. In addition, our low-resolution spectra show strong FeII emission in the UV part (see the following section). [Onoue et al. \(2019\)](#) might not have been able to constrain this component robustly in their fitting due to the low S/N of their data, leading to an over-estimation of the line width. It is also possible that MgII method has overestimated the black hole mass of HSC J2230+0207 due to calibration uncertainties and the differences in BLR properties for this particular system.

The BH mass measurements from $H\alpha$ and $H\beta$ should be relatively reliable given their extensive calibrations; we adopt a final measurement of $M_{\text{BH}} = 3.3 \times 10^8 M_\odot$. The AGN bolometric luminosity can be estimated from the optical continuum as $L_{\text{bol}} = 9.26 \times L_{5100}$ ([Richards et al. 2006](#)) and we have $L_{\text{bol}} \sim 1.9 \times 10^{46}$ erg/s. As a result, the Eddington ratio of this quasar is 0.44^1 , confirming the sub-Eddington accretion status of the SMBH in HSC J2239+0207.

3.2. Proximity Zone

The ages of $z \sim 6$ quasars can be traced by the sizes of their proximity zones where the AGN UV radiation ionizes the surrounding intergalactic medium (IGM) (e.g., [Bolton & Haehnelt 2007](#); [Eilers et al. 2017](#)). These structures are primarily shaped by the history of quasar ionizing radiation and the IGM properties, offering valuable insights into the quasar’s activity duration and its local environment.

To constrain the proximity zone size of HSC J2239+0207, we fitted the quasar continuum at 1241–1285 Å and 1310–1380 Å by a power-law spectrum with a fixed spectral index of $\alpha_\lambda = -1.5$ and assumed the continuum at $\lambda < 1000\text{Å}$ is described by a different power law with $\alpha_\lambda = -0.59$ (i.e., a broken-power model for the AGN continuum; [Shull et al. 2012](#)). The proximity zone size is then determined

by the wavelength difference between the $\text{Ly}\alpha$ wavelength (1215.7 Å) and where the observed flux drops below 10% of the continuum level. (see the top panel of Figure 3)

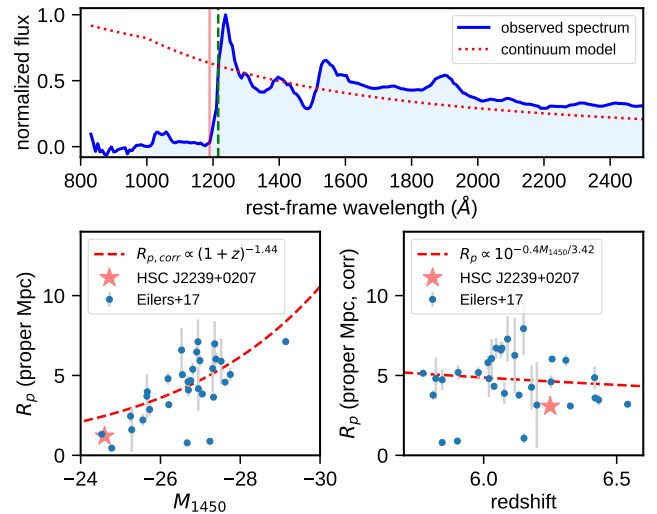


Figure 3. Top panel: continuum-normalized spectrum of HSC J2239+0207. The dashed green vertical line denotes the $\text{Ly}\alpha$ wavelength (1215.7Å) and the pink vertical line denotes the wavelength where the quasar flux (blue line) starts to drop below 10% of the quasar continuum (red dotted line). The wavelength difference between the two ($\delta\lambda$) gives the size of quasar proximity zone. Bottom panels: the location of HSC J2239+0207 on the proximity zone vs AGN luminosity (left) and redshift (right) plane, in comparison to the sample in [Eilers et al. \(2017\)](#). Dashed lines are the best-fit correlations reported in [Eilers et al. \(2017\)](#).

We found a $\delta\lambda \sim 24$ Å, corresponding to a comoving size of 8.8 Mpc or a proper size of 1.2 pMpc at $z = 6.25$. Based on higher resolution ($R \sim 1500$) spectrum and more sophisticated method, [Ishimoto et al. \(2020\)](#) reported a value of 1.65 pMpc for the same quasar. Considering the typical uncertainties of the measured proximity zone sizes (e.g., [Eilers et al. 2017](#)) and the different data and methods, these values are in good agreement. As shown in the bottom panels of Figure 3, HSC J2239+0207 follows the trends defined by other $z \sim 6$ bright quasars ([Eilers et al. 2017](#)). A similar conclusion is also reached by [Ishimoto et al. \(2020\)](#).

From its bolometric luminosity of 1.9×10^{46} erg/s, the corresponding ionizing photon production rate Q_H can be estimated to be $\sim 3.5 \times 10^{56}$ photons/s by adopting a typical UV bolometric luminosity (~ 4 ; [Richards et al. 2006](#)) and ionizing energy $\langle h\nu \rangle \sim 13.6$ eV. The quasar lifetime, t_Q , can be approximated based on the relationship between the size of the proximity zone ($R_p \sim 1.2$ Mpc for this quasar) and the quasar’s ionization history by the following equation

$$t_Q \sim \frac{4\pi R_p^3 n_H}{3Q_H}, \quad (3)$$

¹ or lower if we use the alternative black hole mass estimates

Assuming the surrounding IGM neutral hydrogen number density $n_H \sim 10^{-4} \text{cm}^{-3}$, which is typical for $z \sim 6$ (Bolton & Haehnelt 2007; Eilers et al. 2017), we have a quasar lifetime $t_Q \sim 2$ Myr. In real life, the situation is far more complicated, and the estimated value here should be treated as order-of-magnitude (see discussions in e.g., Eilers et al. 2017). This result reflects the duration of the current active phase during which HSC J2239+0207 has ionized its surrounding IGM. The proximity zone size, being consistent with the luminosity of the quasar, suggests no evidence of an unusually young quasar or an atypically small ionized region. Instead, the quasar must have been active long enough to ionize its surrounding IGM to a typical extent for its luminosity.

3.3. Iron Emission

Iron emission in quasars provide insights into the metallicity and chemical enrichment of the broad-line regions (BLRs), shedding light on the evolutionary stage of these systems.

Following Dietrich et al. (2002), the UV Fe II emission was quantified by integrating the fitted Fe II template at rest-frame 2200–3090 Å. Combining it with the measured flux of the broad Mg II line, we get a flux ratio of Fe II/Mg II ~ 3.66 . This value is consistent with those in other high-redshift quasars, such as those in the XQR-30 sample (Jiang et al. 2024), indicating that HSC J2239+0207 is metal-rich.

In the optical band, following Shen & Ho (2014), we characterize the Fe II strength $R_{\text{Fe II}} = \text{EW}_{\text{Fe II}}/\text{EW}_{\text{H}\beta}$, where the Fe II EW is calculated for the flux within 4434–4684 Å and H β is only for the broad component. The derived $R_{\text{Fe II}} \sim 1.27$ places this quasar within Population A on the quasar main sequence (e.g., Marziani et al. 2018), characterized by relatively high Fe II emission and moderate H β line width (We measure $\text{FWHM}(\text{H}\beta) \sim 3019$ km/s for HSC J2239+0207). Compared to the optical Fe II properties of the eight bright $z \gtrsim 6$ quasars observed by the ASPIRE program (Yang et al. 2023), our quasar presents no notable differences despite its lower AGN luminosity, indicating that HSC J2239+0207 shares typical quasar metallicity without evidence of a particularly young or low-metallicity BLR.

3.4. Winds and Outflows

As shown in the comparison to the standard quasar template, HSC J2239+0207 presents absorption troughs in the rest-frame far-UV, indicating the presence of broad-absorption line (BAL) features. To quantify the BAL strengths, we constrain the balnicity index (BI; Weymann et al. 1991), a modified equivalent width of the BAL absorption, following Bischetti et al. (2023):

$$BI = \int_0^{\nu_{\text{lim}}} \left(1 - \frac{f(\nu)}{0.9} \right) C d\nu, \quad (4)$$

where ν is velocity and $f(\nu)$ is the normalized spectrum, with $C = 1$ only when $f(\nu) < 0.9$, otherwise $C = 0$. The $f(\nu) < 0.9$ limit requires any BAL feature to fall at least 10% below the continuum. We also identify the minimum and maximum velocity, ν_{min} and ν_{max} , for a given transition as the lowest and highest BAL velocity where $C = 1$. The BI is calculated by normalizing the spectrum of HSC J2239 by the quasar template to match the right wing of C IV profile. The results can be seen in Figure 4. For C IV, we get $\nu_{\text{min}} \sim 6000$ km/s, $\nu_{\text{max}} \sim 20900$ km/s and $BI \sim 2700$ km/s. A similar absorption trough is evident in the CIV spectrum of Onoue et al. (2019), with velocity offset and width consistent with the values obtained from the NIRSpect data. For Si IV, we have $\nu_{\text{min}} \sim 3900$ km/s, $\nu_{\text{max}} \sim 18500$ km/s and $BI \sim 1200$ km/s. These large velocity ranges, combined with values of BI, indicate the existence of active, high-energy quasar winds in this system.

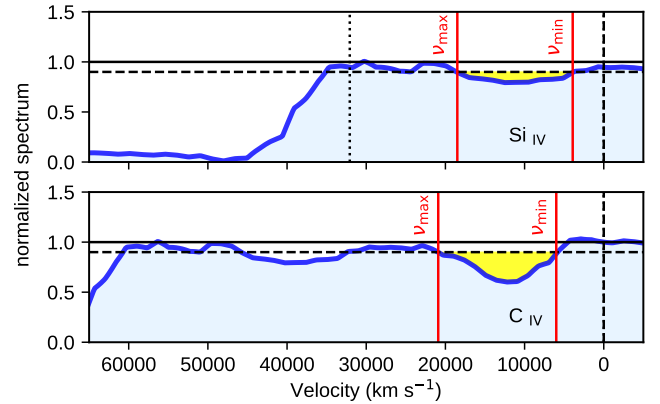


Figure 4. Normalized spectrum of HSC J2239+0207 for the BAL feature measurements. The x-axis indicates the velocity relative to the rest-frame wavelength of the ionic species indicated by the label. The solid (dashed) horizontal line represents a normalized flux level of 1.0 (0.9). BAL troughs defined as normalized flux < 0.9 are highlighted as yellow shaded regions. Vertical red solid lines indicate ν_{max} and ν_{min} for each BAL.

Meanwhile, the profile of the optical H α + [N II] complex shows some asymmetry with a relatively weak blue-shifted component (see the bottom panel in Figure 2). If this is from the H-alpha component, we estimate a velocity offset of ~ 4700 km/s from the blue-shifted broad component, a value consistent with the minimum BAL velocities. This feature may also be associated with the outflows or winds launched near the quasar in HSC J2239.

3.5. Dust Attenuation

From the spectral decomposition, we have derived a Balmer Decrement $(\text{H}\alpha/\text{H}\beta)_{\text{obs}} = 2.51 \pm 0.2$ for the quasar broad-line regions, a value consistent with the ratios observed

for the bluest quasars ($\sim 2.72 \pm 0.04$) at low- z (Gaskell 2017). In addition, as seen in Figure 1, the quasar UV-to-optical continuum is in excellent agreement with the blue quasar template once the variations of Fe II emission are considered. These observations suggest that the quasar does not have much dust reddening along the polar direction and indicate the dearth of small grains that cause the UV-optical dust extinction.

3.6. Host Galaxy

As described in Stone et al. (2023), NIRC*am* images of J2239+0207 show the quasar host galaxy is very compact with an effective radius of ~ 1 kpc, corresponding to $\sim 0.17''$. We have not detected any extended host signals at the quasar location from the datacube, which is expected given the limited spatial resolution of NIRS*pec* IFU ($0.1'' \times 0.1''$ for every spatial pixel) and the more complicated instrument PSF. The unresolved quasar spectrum still provides the opportunity to decompose the integrated light into an AGN and a galaxy component. We do not detect an obvious host signal with PyQSOFit, likely because of the poor spectral resolution of the prism does not allow reliable measurements of the weak stellar absorption lines and the spectral fitting is dominated by broad features such as strong iron emission and quasar power-law continuum.

The spectrum is better-suited for characterizing broad features, such as the Balmer break. In Figure 1, we have compared the spectrum of J2239+0207 to the quasar template with minimal host galaxy contamination. Besides the obviously stronger Iron emission features and the absorption in the UV, they are identical, suggesting the host galaxy contribution of J2239+0207 is indeed very weak, consistent with the an undermassive host galaxy revealed from NIRC*am* observations (Stone et al. 2023). Motivated by the stellar mass constrained with NIRC*am* from Stone et al. (2023) and the measured host stellar populations of similar quasars by Onoue et al. (2024), we have computed a model galaxy spectrum with a stellar mass of $10^{10} M_{\odot}$ at $z=6.25$ with Flexible Stellar Population Synthesis (FSPS; Conroy et al. 2009; Conroy & Gunn 2010) assuming a delayed- τ star formation history with e-folding time of 20 Myr, stellar age of 200 Myr and attenuation level $A_V = 0.1$ and plot it together with the scaled quasar template. As shown by the dotted line in Figure 1, the contribution of such a host galaxy would be minimal to the integrated quasar light, fully consistent with the lack of a stellar component in the PyQSOFit spectral decomposition results.

4. A GAS COMPANION

As shown in Figure 5, near the [O III] and the (unresolved) [N II]+H α wavelengths of the IFU data cube, we have identified an emission-line companion at an angular separation of

~ 1 arcsec to the quasar without a significant continuum detection from the UV to the optical. At the quasar redshift, this companion has a projected distance of approximately 5 kpc to the quasar. Spatially, it is slightly elongated towards the quasar radial direction with a size of $0.6'' \times 1''$, corresponding to a physical extent of $\sim 3 \times 5$ kpc at the quasar redshift.

On the middle panel of Figure 5, we show the extracted 1-D spectrum of the companion and compared it to the quasar spectrum. A few lines are detected for this companion, including the [O III] $\lambda\lambda$ 5007, 4959 and the unresolved H α + [N II] complex. The H β emission line is not convincingly detected. and the strength of H α emission can also not be separated from that of [N II], due to the limited spectral resolution. Compared to the quasar spectrum, all these lines are shifted towards longer wavelengths. We find that the [O III] emission lines of this gas companion are red-shifted relatively to those from the quasar by $0.0144 \pm 0.0008 \mu\text{m}$ in the observed frame, corresponding to a velocity offset of $\sim 1200 \pm 200$ km/s at $z = 6.25$ (with both the measurement uncertainty and the spectral resolution considered).

By fitting the spectral lines with one single Gaussian function, we find the integrated line strength of the [O III] doublet is $I_{[\text{OIII},5007]} \sim 4.9 \times 10^{-18}$ erg/cm 2 /s (11σ) and $I_{[\text{OIII},4959]} \sim 1.6 \times 10^{-18}$ erg/cm 2 /s (6σ). The H β emission line is not detected with a 3σ upper limit of $I_{H\beta} \lesssim 4.6 \times 10^{-19}$ erg/cm 2 /s. The H α + [N II] emission is unresolved in the prism spectrum with a total line strength about 4.0×10^{-18} erg/cm 2 /s (6σ). Assuming the gas companion does not have extinction in the optical with an intrinsic ratio $I_{H\alpha}/I_{H\beta} = 2.86$, we can put an upper limit of H α flux, $I_{H\alpha} \lesssim 1.3 \times 10^{-18}$ erg/cm 2 /s, making the [N II] emission contribute more than half of the unresolved flux. Also note the ratio between the [N II] doublets $I_{\text{NII},6583}/I_{\text{NII},6549} = 3.0$, we can infer the $I_{\text{NII},6583} \gtrsim 2.0 \times 10^{-18}$ erg/cm 2 /s and $I_{\text{NII},6549} \gtrsim 0.7 \times 10^{-18}$ erg/cm 2 /s. The corresponding flux ratios [N II,6583]/H $\alpha \gtrsim 1.5$ and [O III,5007]/H $\beta \gtrsim 10$. These values would put the system into the AGN-dominated area in the classical BPT diagram and can be produced by either AGN hard radiation (for relatively low ratios) or shocks (for the extreme ratios) (e.g., D'Agostino et al. 2019)

Besides some faint signals in the NIRC*am* F360M image likely associated with the [O III] emission (see the zoom-in panel in Figure 1 of Stone et al. 2023), we do not detect any emission at the companion location in F210M, F480M and have put a $3\text{-}\sigma$ upper limit on its stellar mass of $4 \times 10^9 M_{\odot}$, following a similar strategy in Stone et al. (2023). In addition, ALMA observations of HSC J2239+0207 presented by Izumi et al. (2019) neither reported any [C II] flux nor cold dust continuum at the location of this gas companion.

We will discuss the nature of this companion and its possible relation to the quasar in Section 5.2.

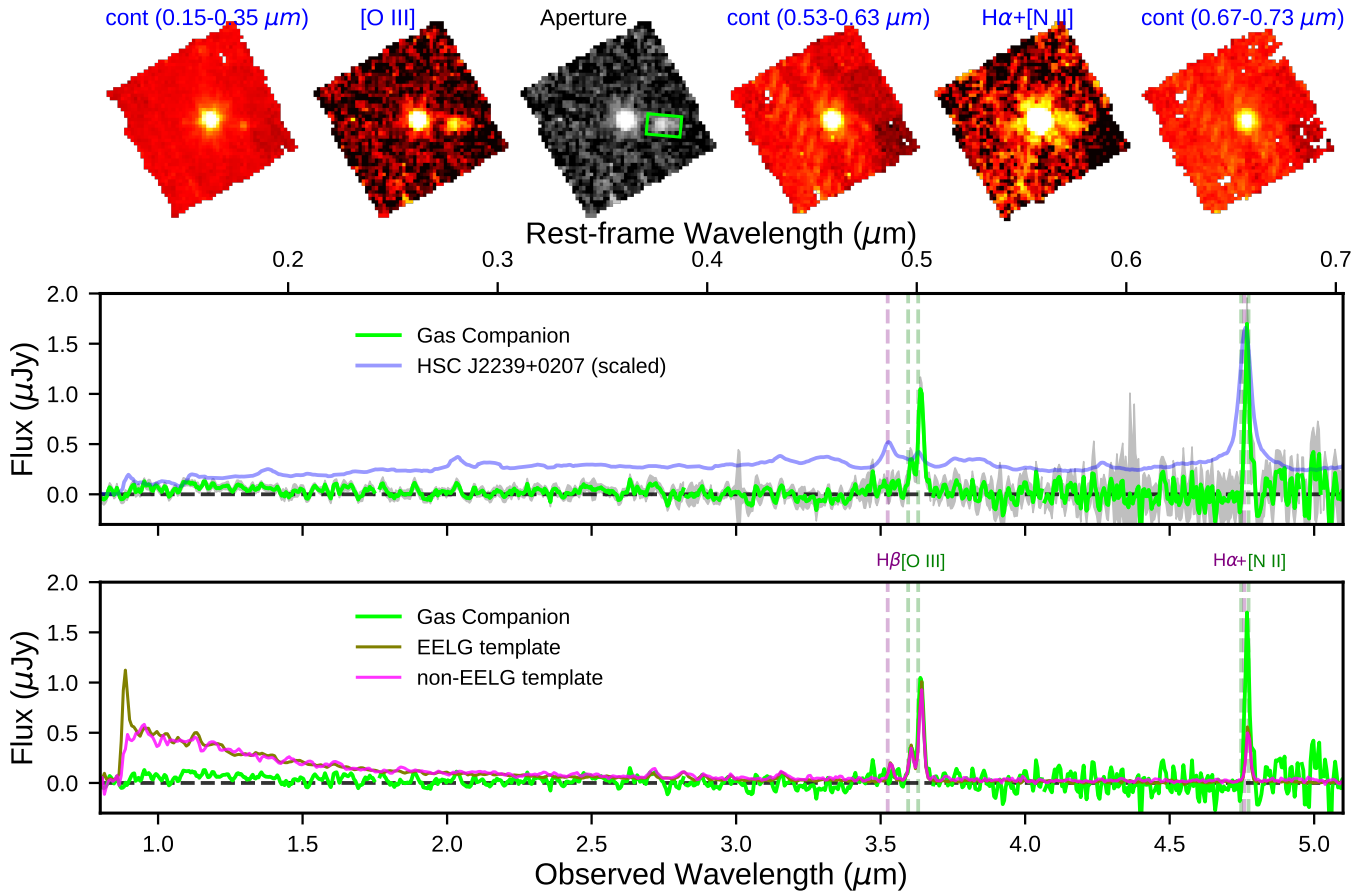


Figure 5. Top panel: The IFU re-constructed images of the quasar HSC J2239+0207. The post-stamps show images at the flux peak of the [OIII] and H α + [N II] emission as well as the adjacent emission-line-free continuum. We have highlighted the rectangular aperture used to extract the companion signals in green. Middle panel: The NIRSpec IFU prism spectra of the emission companion (green line) with the 1σ uncertainties (gray shaded regions). We also plot the observed spectrum of quasar HSC J2239+0207 as a comparison (blue line) and labeled the [OIII], H β , [N II], and H α wavelengths at the quasar redshift. Bottom panel: The NIRSpec IFU prism spectra of the companion (green line) compared to two stacked spectra for extreme emission line galaxies (EELGs; dark yellow line) and non-EELGs (magenta line) at $z > 5.7$ from Boyett et al. (2024).

5. DISCUSSION

5.1. HSC J2239+0207 – A Possibly Fading Quasar

HSC J2239+0207 provides a unique opportunity to study the evolution of quasars during the epoch of reionization. Its sub-Eddington accretion rate ($\lambda_{\text{Edd}} \sim 0.4$) sets it apart from the majority of bright quasars at $z \sim 6$, which typically accrete near or above the Eddington limit (e.g., Inayoshi et al. 2020). This lower accretion rate, combined with its over-massive SMBH ($M_{\text{BH}} \sim 3.3\text{--}3.5 \times 10^8 M_{\odot}$) relative to its compact and undermassive host galaxy (Stone et al. 2023), suggests the system has undergone an earlier period of rapid SMBH growth and is now entering a less active phase, during which the host galaxy may grow to bring the system closer to the local $M_{\text{BH}}\text{--}M_*$ relation.

The estimated lifetime of the quasar stage, on the order of 1 Myr, is inferred from its proximity size of 1.2 proper Mpc

(see Section 3.2). This highlights the relatively short duration of its recent active phase. This lifetime falls towards the lower end of quasar lifetimes estimated from proximity zones, typically $10^5\text{--}10^7$ years (e.g., Eilers et al. 2017), suggesting the quasar has not been persistently active throughout its history. Instead, the proximity zone is consistent with the luminosity of the quasar, implying sufficient activity to ionize its surrounding IGM but not beyond what is typical for its energy output.

The spectral characteristics of HSC J2239+0207 further support this interpretation. The strong Fe II emission and typical proximity zone size indicate a metal-rich, highly evolved system that has likely been active overall for a significant duration, presumably in a series of high-activity periods. These properties are in contrast to young quasars or young AGNs, which often show smaller proximity zones (Eilers et al. 2020) or significantly reduced Fe II emission (Trefoloni et al. 2024).

In addition, the presence of high-velocity BALs in the UV spectrum of HSC J2239+0207, indicative of powerful outflows, along with minimal dust reddening in the polar direction, suggests that AGN feedback has regulated the evolution of the SMBH and its environment, potentially clearing the available accretion material along certain sight lines.

However, while the evidence points toward declining activity, the term “fading” must be interpreted cautiously. The sub-Eddington accretion could reflect a temporary depletion of fuel rather than a permanent transition to quiescence. Furthermore, the quasar remains luminous and active, with feedback processes continuing to shape its surroundings, as evidenced by the detection of a gas companion with high ionization ratios ($[\text{O III}]/\text{H}\beta \gtrsim 10$) likely driven by AGN radiation or shocks (see next Section).

5.2. Nature of the Gas Companion

The gas companion observed near HSC J2239+0207, located at a projected distance of ~ 5 kpc, presents several intriguing characteristics. It exhibits strong $[\text{O III}]$ and $\text{H}\alpha + [\text{N II}]$ emission without notable continuum emission from UV to the optical. The high $[\text{O III}]/\text{H}\beta$ ratio ($\gtrsim 10$) places the system in the AGN-dominated region of the classical BPT diagram, suggesting that the ionization is driven by AGN hard radiation or shocks rather than star formation. The salient features that guide any discussion are: (1) the ratio of $\text{H}\alpha + [\text{N II}]$ to $\text{H}\beta$ of $\gtrsim 8$; (2) the large extent of the $\text{H}\alpha + [\text{N II}]$ emission, of order 4 kpc; and (3) the lack of strong UV continuum emission. Explaining these characteristics is challenging and the true nature of this companion remains ambiguous, with several possible interpretations considered below.

One possibility is that the companion is an isolated high-redshift emission-line galaxy. At similar redshifts, a large population of young galaxies are known to show strong nebular emission, particularly bright $[\text{O III}]$ lines, at similar redshifts (e.g., Tang et al. 2023; Boyett et al. 2024). In the bottom panel of Figure 5, we have compared the spectral templates of such galaxies from Boyett et al. (2024) to the spectrum of this companion. If we match the $[\text{O III}]$ line profiles of the companion, these galaxy templates can explain the lack of stellar continuum emission in the rest-frame optical wavelengths reasonably well, but two notable differences are revealed. First, despite the weaker optical stellar emission, these high- z galaxies typically present strong UV continuum emission from young stars while this companion does not show a significant detection. Second, the strength of $\text{H}\alpha + [\text{N II}]$ complex from the companion is atypical compared with that in the high- z star-forming galaxies. Consequently, this scenario not likely.

Another possibility is that we are seeing a galaxy in the initial stages of merging with the quasar/host galaxy system.

The free-fall velocity assuming a quasar mass of $2.9 \times 10^{11} M_{\odot}$ (Izumi et al. 2019) is $\sim 700 \text{ km s}^{-1}$, which is consistent with the velocity difference from the quasar if the latter has a small velocity of its own in our direction. In this situation, we expect the ISM of the merging galaxy to be characterized by emission in shocks. This hypothesis provides a straightforward explanation for the strong $\text{H}\alpha + [\text{N II}]$ emission, since the ISM in merging or interacting galaxies is shocked and the $[\text{N II}]$ lines are significantly enhanced (e.g., Rich et al. 2015; Mortazavi & Lotz 2019), up to being comparable to $\text{H}\alpha$, i.e., the observed value would be compatible with $\text{H}\alpha/\text{H}\beta \sim 3$. The largest caution about this hypothesis is that the dynamical mass is quite uncertain due to the effect of the inclination angle on the circum-quasar gas, and that accounting for the large velocity difference is therefore in question. In addition, observations of quasar-galaxy mergers at similar redshifts reveal substantial stellar masses and rest-frame UV emission due to enhanced star formation during the merging process (e.g., Decarli et al. 2019), which are missing in the companion.

A third scenario is that the gas companion represents tidally disrupted material from a galaxy passing by. To evaluate this possibility, we estimate the quasar’s halo mass using the empirical relation for galaxies at $z \sim 6$ in Behroozi et al. (2013) and find $M_{\text{halo}} \sim 4 \times 10^{11} M_{\odot}$ for the host galaxy’s stellar mass $\sim 10^{10} M_{\odot}$ (Stone et al. 2023). Adopting the Navarro-Frenk-White (NFW) profile, the halo’s virial radius, R_{vir} , is given by

$$R_{\text{vir}} \sim \left(\frac{3M_{\text{halo}}}{4\pi\Delta_c\rho_{\text{crit}}} \right)^{1/3}, \quad (5)$$

where $\Delta_c = 200$ for virialized structures and ρ_{crit} is the critical density of the Universe at $z \sim 6.25$. This calculation yields $R_{\text{vir}} \sim 14$ kpc, indicating that the gas companion is within the halo if it shares the quasar redshift. Assuming the NFW profile, the escape velocity at 5 kpc is about 200 km/s. However, the redshifted $[\text{O III}]$ emission of this gas companion indicates a velocity offset of ~ 1200 km/s relative to the quasar, far exceeding this escape velocity. This makes the tidal disruption scenario unlikely.

A more compelling interpretation is that the gas companion is associated with AGN-driven outflows. The high velocity, elongated morphology, and alignment along the quasar’s radial direction suggest that it may represent outflowing gas propelled by AGN feedback. The strong BAL features in the quasar’s UV spectrum indicate powerful winds, and the companion could be a larger-scale manifestation of these feedback processes. Collimated outflows or shocks may have shaped the observed structure and sustained the high ionization observed in the gas, as suggested in e.g., D’Agostino et al. (2019).

The companion could be analogous to low-redshift “quasar ionization echoes,” such as Hanny’s Voorwerp (Lintott et al. 2009). In this scenario, the gas cloud could represent material ionized by the quasar’s past activity, potentially stripped from the host galaxy or another source. However, the compact and elongated morphology of this companion suggests a more dynamic origin, such as outflowing gas pushed away by the AGN wind rather than a static ionization remnant.

In conclusion, the properties of the gaseous quasar companion suggest a variety of interesting explanations, possibly favoring an origin tied to AGN-driven feedback. Future deeper JWST NIRCам and high-resolution NIRSspec observations will be critical for disentangling these scenarios, providing a definitive understanding of the role of AGN feedback in shaping the environment of HSC J2239+0207 during the epoch of reionization.

5.3. Implication on the SMBH Growth and BH-Galaxy Co-evolution

HSC J2239+0207 offers valuable insights into the complex interplay between SMBH growth and host galaxy evolution during the epoch of reionization. This quasar exhibits strong BAL features indicative of significant gas outflows, yet shows no evidence of dust reddening in its UV-optical continuum or broad-line Balmer decrement. One possible explanation is that AGN feedback, through mechanisms such as hard radiation or shocks, has effectively removed the relatively small dust grains responsible for the UV-optical extinction along the polar direction (e.g., Laor & Draine 1993; Tazaki & Ichikawa 2020). Under this framework, the gas companion identified near the quasar may also represent a remnant of earlier feedback activity.

At longer wavelengths, ALMA observations reveal that the host galaxy of HSC J2239+0207 is an ultraluminous infrared galaxy (ULIRG) with $L_{\text{IR}} \sim 2.2 \times 10^{12} L_{\odot}$, corresponding to a star formation rate of $\sim 450 M_{\odot} \text{yr}^{-1}$ (Izumi et al. 2019). Compared to the compact far-IR dust continuum (FWHM $\sim 1.2 \text{ kpc} \times 0.7 \text{ kpc}$), its [C II] emission is extended (FWHM $\sim 4.0 \text{ kpc} \times 2.6 \text{ kpc}$) with filamentary structures that trace the existence of a cold interstellar medium (ISM). Even assuming $\sin i = 1$, the indicated mass, $6.4 \pm 1.3 \times 10^{10} M_{\odot}$, significantly exceeds the mass attributed to the host galaxy, implying an exceptionally large mass for this material. Considering the observations presented in this work, we suggest that although the cold ISM remains available to sustain star formation, AGN feedback from the quasar has inhibited the growth of the host galaxy, resulting in an under-massive host stellar component compared to the SMBH (Stone et al. 2023).

Very recently, Onoue et al. (2024) reported the JWST/NIRSspec fixed slit spectra of two other HSC quasars (J2236+0032 and J1512+4422), showing post-starburst sig-

natures in their host galaxies, and suggested that the star formation activities were recently quenched by the AGN feedback. Although we do not have direct spectral constraints on the host galaxy stellar population for HSC J2239+0207 due to the lack of spectral resolution and the fainter host galaxy signals, HSC J2239+0207 may follow the same evolutionary path as J2236+0032 and J1512+4422, with the AGN feedback strongly regulating the galaxy growth.

6. SUMMARY

In this paper, we have presented the NIRSspec/IFU prism observations of HSC J2239+0207, a low-luminosity quasar at $z \sim 6.25$. Despite the low spectral resolution of the prism data, we have provided various constraints on the quasar properties and reported a discovery of a gas companion near the quasar redshift. Our major findings are:

- The mass of the SMBH in this system is estimated to be $(3.3\text{--}3.5) \times 10^8 M_{\odot}$ from the $\text{H}\alpha$ and $\text{H}\beta$ broad emission lines and the corresponding Eddington ratio is 0.44. In contrast to other bright quasars accreting at or above Eddington limit, HSC J2239+0207 is in a less active phase;
- We estimate HSC J2239+0207 has a proximity zone size of 1.2 proper Mpc, consistent with its luminosity and suggesting a recent active phase of on the order of 1 Myr. This short lifetime places the quasar at the lower end of proximity zone-derived lifetimes observed in $z \sim 6$ quasars, indicating that this quasar is transitioning out of its peak activity phase;
- Consistent with other high-redshift bright quasars, HSC J2239+0207 has strong iron emission and identical spectral properties to its low- z counterparts, indicating the system is metal-rich and highly evolved and it must have experienced a period (or periods) of active SMBH growth in the past;
- There are strong BAL features in the UV part of the spectrum that trace strong AGN-driven winds along the line of sight. However, little dust reddening is revealed from the broad Balmer decrement and the quasar UV-to-optical continuum. AGN feedback such as hard radiation or shocks can remove the dust grains along the polar direction and explain these observations;
- We find a gas companion at a distance of ~ 1 arcsec to the quasar without notable UV-optical continuum emission but a high $[\text{O III}]/\text{H}\beta$ ratio and possibly extreme $[\text{N II}]$ emission line strength, indicating the ionization from an AGN or shocks. Although we cannot completely rule out other possibilities, considering

various constraints, the most favorable explanation for this companion is that this gas cloud was blown away by the quasar feedback from the host ISM at some earlier time.

Combined with previous NIRC*am* study of this quasar by Stone et al. (2023), we have revealed that HSC J2239+0207 is a sub-Eddington quasar with an under-massive host galaxy and a gas companion. The AGN feedback traced by the strong BAL features in the UV is the most reasonable explanation for the slower growth of the host galaxy despite the rich cold gas reserve revealed by ALMA, as well as the origin and the high-ionization nature of the gas companion and the lack of dust reddening of the quasar along the polar direction reported in this work.

This object provides a unique opportunity to study the subsequent evolution of bright quasars in the reionization epoch and offers valuable insights into the interplay between SMBH growth, the host galaxy evolution and the surrounding environment in the early Universe. Future JWST obser-

vations with improved spectral resolution and sensitivity are desired to enable further study of this intriguing system.

We thank Dr. Kit Boyett for providing a digital copy of the stacked emission-line galaxy spectra published in Boyett et al. (2024). J.L., G.R. M.S. and S.A. acknowledge support from the JWST Mid-Infrared Instrument (MIRI) grant No. 80NSSC18K0555, and the NIRC*am* science support contract NAS5-02105, both from NASA Goddard Space Flight Center to the University of Arizona. The JWST data presented in this paper were obtained from the Mikulski Archive for Space Telescopes (MAST) at the Space Telescope Science Institute.

Facilities: JWST(NIRC*am*, NIRS*pec*)

Software: Astropy (Astropy Collaboration et al. 2018), Matplotlib (Hunter 2007), NumPy (Harris et al. 2020), SciPy (Virtanen et al. 2020), WebbPSF (Perrin et al. 2014), PyQSOFit (Guo et al. 2018)

REFERENCES

- Alexander, D. M., & Hickox, R. C. 2012, *NewAR*, 56, 93, doi: [10.1016/j.newar.2011.11.003](https://doi.org/10.1016/j.newar.2011.11.003)
- Astropy Collaboration, Price-Whelan, A. M., Sipőcz, B. M., et al. 2018, *AJ*, 156, 123, doi: [10.3847/1538-3881/aabc4f](https://doi.org/10.3847/1538-3881/aabc4f)
- Behroozi, P. S., Wechsler, R. H., & Conroy, C. 2013, *ApJ*, 770, 57, doi: [10.1088/0004-637X/770/1/57](https://doi.org/10.1088/0004-637X/770/1/57)
- Bischetti, M., Fiore, F., Feruglio, C., et al. 2023, *ApJ*, 952, 44, doi: [10.3847/1538-4357/accea4](https://doi.org/10.3847/1538-4357/accea4)
- Bolton, J. S., & Haehnelt, M. G. 2007, *MNRAS*, 382, 325, doi: [10.1111/j.1365-2966.2007.12372.x](https://doi.org/10.1111/j.1365-2966.2007.12372.x)
- Boroson, T. A., & Green, R. F. 1992, *ApJS*, 80, 109, doi: [10.1086/191661](https://doi.org/10.1086/191661)
- Boyett, K., Bunker, A. J., Curtis-Lake, E., et al. 2024, arXiv e-prints, arXiv:2401.16934, doi: [10.48550/arXiv.2401.16934](https://doi.org/10.48550/arXiv.2401.16934)
- Conroy, C., & Gunn, J. E. 2010, *ApJ*, 712, 833, doi: [10.1088/0004-637X/712/2/833](https://doi.org/10.1088/0004-637X/712/2/833)
- Conroy, C., Gunn, J. E., & White, M. 2009, *ApJ*, 699, 486, doi: [10.1088/0004-637X/699/1/486](https://doi.org/10.1088/0004-637X/699/1/486)
- D'Agostino, J. J., Kewley, L. J., Groves, B. A., et al. 2019, *MNRAS*, 487, 4153, doi: [10.1093/mnras/stz1611](https://doi.org/10.1093/mnras/stz1611)
- Decarli, R., Dotti, M., Bañados, E., et al. 2019, *ApJ*, 880, 157, doi: [10.3847/1538-4357/ab297f](https://doi.org/10.3847/1538-4357/ab297f)
- Dietrich, M., Hamann, F., Shields, J. C., et al. 2002, *ApJ*, 581, 912, doi: [10.1086/344410](https://doi.org/10.1086/344410)
- Ding, X., Onoue, M., Silverman, J. D., et al. 2023, *Nature*, 621, 51, doi: [10.1038/s41586-023-06345-5](https://doi.org/10.1038/s41586-023-06345-5)
- Eilers, A.-C., Davies, F. B., Hennawi, J. F., et al. 2017, *ApJ*, 840, 24, doi: [10.3847/1538-4357/aa6c60](https://doi.org/10.3847/1538-4357/aa6c60)
- Eilers, A.-C., Hennawi, J. F., Decarli, R., et al. 2020, *ApJ*, 900, 37, doi: [10.3847/1538-4357/aba52e](https://doi.org/10.3847/1538-4357/aba52e)
- Eilers, A.-C., Mackenzie, R., Pizzati, E., et al. 2024, *ApJ*, 974, 275, doi: [10.3847/1538-4357/ad778b](https://doi.org/10.3847/1538-4357/ad778b)
- Fan, X., Bañados, E., & Simcoe, R. A. 2023, *ARA&A*, 61, 373, doi: [10.1146/annurev-astro-052920-102455](https://doi.org/10.1146/annurev-astro-052920-102455)
- Gaskell, C. M. 2017, *MNRAS*, 467, 226, doi: [10.1093/mnras/stx094](https://doi.org/10.1093/mnras/stx094)
- Greene, J. E., & Ho, L. C. 2005, *ApJ*, 630, 122, doi: [10.1086/431897](https://doi.org/10.1086/431897)
- Guo, H., Shen, Y., & Wang, S. 2018, PyQSOFit: Python code to fit the spectrum of quasars, Astrophysics Source Code Library. <http://ascl.net/1809.008>
- Harris, C. R., Millman, K. J., van der Walt, S. J., et al. 2020, *Nature*, 585, 357, doi: [10.1038/s41586-020-2649-2](https://doi.org/10.1038/s41586-020-2649-2)
- Heckman, T. M., & Best, P. N. 2014, *ARA&A*, 52, 589, doi: [10.1146/annurev-astro-081913-035722](https://doi.org/10.1146/annurev-astro-081913-035722)
- Hopkins, P. F., Hernquist, L., Cox, T. J., & Kereš, D. 2008, *ApJS*, 175, 356, doi: [10.1086/524362](https://doi.org/10.1086/524362)
- Hunter, J. D. 2007, *Computing in Science and Engineering*, 9, 90, doi: [10.1109/MCSE.2007.55](https://doi.org/10.1109/MCSE.2007.55)
- Inayoshi, K., Visbal, E., & Haiman, Z. 2020, *ARA&A*, 58, 27, doi: [10.1146/annurev-astro-120419-014455](https://doi.org/10.1146/annurev-astro-120419-014455)
- Ishimoto, R., Kashikawa, N., Onoue, M., et al. 2020, *ApJ*, 903, 60, doi: [10.3847/1538-4357/abb80b](https://doi.org/10.3847/1538-4357/abb80b)
- Izumi, T., Onoue, M., Matsuoka, Y., et al. 2019, *PASJ*, 71, 111, doi: [10.1093/pasj/psz096](https://doi.org/10.1093/pasj/psz096)

- Jiang, D., Onoue, M., Jiang, L., et al. 2024, *ApJ*, 975, 214, doi: [10.3847/1538-4357/ad7d09](https://doi.org/10.3847/1538-4357/ad7d09)
- Kormendy, J., & Ho, L. C. 2013, *ARA&A*, 51, 511, doi: [10.1146/annurev-astro-082708-101811](https://doi.org/10.1146/annurev-astro-082708-101811)
- Laor, A., & Draine, B. T. 1993, *ApJ*, 402, 441, doi: [10.1086/172149](https://doi.org/10.1086/172149)
- Lintott, C. J., Schawinski, K., Keel, W., et al. 2009, *MNRAS*, 399, 129, doi: [10.1111/j.1365-2966.2009.15299.x](https://doi.org/10.1111/j.1365-2966.2009.15299.x)
- Marziani, P., Dultzin, D., Sulentic, J. W., et al. 2018, *Frontiers in Astronomy and Space Sciences*, 5, 6, doi: [10.3389/fspas.2018.00006](https://doi.org/10.3389/fspas.2018.00006)
- Matsuoka, Y., Strauss, M. A., Kashikawa, N., et al. 2018, *ApJ*, 869, 150, doi: [10.3847/1538-4357/aaee7a](https://doi.org/10.3847/1538-4357/aaee7a)
- Mortazavi, S. A., & Lotz, J. M. 2019, *MNRAS*, 487, 1551, doi: [10.1093/mnras/stz1331](https://doi.org/10.1093/mnras/stz1331)
- Onoue, M., Kashikawa, N., Matsuoka, Y., et al. 2019, *ApJ*, 880, 77, doi: [10.3847/1538-4357/ab29e9](https://doi.org/10.3847/1538-4357/ab29e9)
- Onoue, M., Ding, X., Silverman, J. D., et al. 2024, arXiv e-prints, arXiv:2409.07113, doi: [10.48550/arXiv.2409.07113](https://doi.org/10.48550/arXiv.2409.07113)
- Perrin, M. D., Sivaramakrishnan, A., Lajoie, C.-P., et al. 2014, in *Society of Photo-Optical Instrumentation Engineers (SPIE) Conference Series*, Vol. 9143, *Space Telescopes and Instrumentation 2014: Optical, Infrared, and Millimeter Wave*, ed. J. Oschmann, Jacobus M., M. Clampin, G. G. Fazio, & H. A. MacEwen, 91433X, doi: [10.1117/12.2056689](https://doi.org/10.1117/12.2056689)
- Rich, J. A., Kewley, L. J., & Dopita, M. A. 2015, *ApJS*, 221, 28, doi: [10.1088/0067-0049/221/2/28](https://doi.org/10.1088/0067-0049/221/2/28)
- Richards, G. T., Lacy, M., Storrie-Lombardi, L. J., et al. 2006, *ApJS*, 166, 470, doi: [10.1086/506525](https://doi.org/10.1086/506525)
- Schneider, D. P., Richards, G. T., Hall, P. B., et al. 2010, *AJ*, 139, 2360, doi: [10.1088/0004-6256/139/6/2360](https://doi.org/10.1088/0004-6256/139/6/2360)
- Shen, Y., & Ho, L. C. 2014, *Nature*, 513, 210, doi: [10.1038/nature13712](https://doi.org/10.1038/nature13712)
- Shull, J. M., Stevans, M., & Danforth, C. W. 2012, *ApJ*, 752, 162, doi: [10.1088/0004-637X/752/2/162](https://doi.org/10.1088/0004-637X/752/2/162)
- Somerville, R. S., & Davé, R. 2015, *ARA&A*, 53, 51, doi: [10.1146/annurev-astro-082812-140951](https://doi.org/10.1146/annurev-astro-082812-140951)
- Stone, M. A., Lyu, J., Rieke, G. H., & Alberts, S. 2023, *ApJ*, 953, 180, doi: [10.3847/1538-4357/acebe0](https://doi.org/10.3847/1538-4357/acebe0)
- Stone, M. A., Lyu, J., Rieke, G. H., Alberts, S., & Hainline, K. N. 2024, *ApJ*, 964, 90, doi: [10.3847/1538-4357/ad2a57](https://doi.org/10.3847/1538-4357/ad2a57)
- Tang, M., Stark, D. P., Chen, Z., et al. 2023, *MNRAS*, 526, 1657, doi: [10.1093/mnras/stad2763](https://doi.org/10.1093/mnras/stad2763)
- Tazaki, R., & Ichikawa, K. 2020, *ApJ*, 892, 149, doi: [10.3847/1538-4357/ab72f6](https://doi.org/10.3847/1538-4357/ab72f6)
- Trefoloni, B., Ji, X., Maiolino, R., et al. 2024, arXiv e-prints, arXiv:2410.21867, doi: [10.48550/arXiv.2410.21867](https://doi.org/10.48550/arXiv.2410.21867)
- Vanden Berk, D. E., Richards, G. T., Bauer, A., et al. 2001, *AJ*, 122, 549, doi: [10.1086/321167](https://doi.org/10.1086/321167)
- Vestergaard, M., & Peterson, B. M. 2006, *ApJ*, 641, 689, doi: [10.1086/500572](https://doi.org/10.1086/500572)
- Vestergaard, M., & Wilkes, B. J. 2001, *ApJS*, 134, 1, doi: [10.1086/320357](https://doi.org/10.1086/320357)
- Virtanen, P., Gommers, R., Oliphant, T. E., et al. 2020, *Nature Methods*, 17, 261, doi: [10.1038/s41592-019-0686-2](https://doi.org/10.1038/s41592-019-0686-2)
- Wang, F., Yang, J., Hennawi, J. F., et al. 2023, *ApJL*, 951, L4, doi: [10.3847/2041-8213/accd6f](https://doi.org/10.3847/2041-8213/accd6f)
- Weymann, R. J., Morris, S. L., Foltz, C. B., & Hewett, P. C. 1991, *ApJ*, 373, 23, doi: [10.1086/170020](https://doi.org/10.1086/170020)
- Yang, J., Wang, F., Fan, X., et al. 2023, *ApJL*, 951, L5, doi: [10.3847/2041-8213/acc9c8](https://doi.org/10.3847/2041-8213/acc9c8)
- Yue, M., Eilers, A.-C., Simcoe, R. A., et al. 2024, *ApJ*, 966, 176, doi: [10.3847/1538-4357/ad3914](https://doi.org/10.3847/1538-4357/ad3914)